arXiv:1511.03094v3 [cond-mat.mes-hall] 25 Jun 2016

Optical signatures of electric field driven magnetic phase transitions in graphene quantum dots

*Tista Basak and $Alok Shukla

*Mukesh Patel School of Technology Management and Engineering, NMIMS University, Mumbai-56, India and
$Department of Physics, Indian Institute of Technology Bombay, Powai, Mumbai-400076, INDIA.*

Experimental challenges in identifying various types of magnetic ordering in graphene quantum dots (QDs) pose a major hurdle in the application of these nanostructures for spintronic devices. Based upon phase diagrams obtained by employing the π-electron Pariser-Parr-Pople (PPP) model Hamiltonian, we demonstrate that the magnetic states undergo phase transition under the influence of an external electric field. Our calculations of the electro-absorption spectra of these QDs indicate that the spectrum in question carries strong signatures of their magnetic state (FM vs AFM), thus suggesting the possibility of an all-optical characterization of their magnetic nature. Further, the gaps for the up and the down spins are the same in the absence of an external electric field, both for the antiferromagnetic (AFM), and the ferromagnetic (FM) states of QDs. But, once the QDs are exposed to a suitably directed external electric field, gaps for different spins split, and, exhibit distinct variations with respect to the strength of the field. The nature of variation exhibited by the energy gaps corresponding to the up and down spins is different for the AFM and FM configurations of QDs. This selective manipulation of the spin-polarized gap splitting by an electric field in finite graphene nanostructures can open up new frontiers in the design of graphene-based spintronic devices.

I. INTRODUCTION

The existence of intrinsic magnetism in graphene is a highly controversial issue which has evoked considerable research interest among the scientific fraternity for the past few years.[1–6] Theoretical studies[1,2,4–17] have revealed that quantum confinement, shape, edge topology, and application of an external electric field have a profound influence on the magnetic properties of graphene-based nanostructures which can be efficiently exploited for designing novel spintronic devices.[18–21] It has been recently predicted that the application of electric field can induce energy-level shifts of spin-ordered edge states resulting in phase transition between the different magnetic states of zigzag-edged graphene nanostructures.[1–3,5,6] Further, it was revealed that in case of the antiferromagnetic (AFM) phase of graphene nanostructures, the applied electric field breaks the spin degeneracy leading to half-semiconducting behavior.[3] Although a number of theoretical calculations probing magnetism in regular shaped graphene quantum dots (QDs) have been performed, very little literature exists on such studies of irregular shaped QDs.[22] Recently, Chen *et al.*,[22] provided experimental evidence of intrinsic magnetism in graphene sheets with irregular zigzag edges. However, indisputable experimental evidence to corroborate various theoretical predictions is still lacking due to the complications involved in precision measurements of weak magnetic signals in graphene nanostructures by employing current techniques.[22–25] This has inspired us to look at other options to solve this problem, and in an earlier work,[26] we had analyzed an all-optical technique based upon electroabsorption (EA) spectra to efficiently detect the magnetic ground state of one-dimensional structures, *viz.*, graphene nanoribbons. In this work, we investigate the use of EA spectroscopy to probe different magnetic configurations of zero-dimensional graphene structures, i.e., QDs. Employing a correlated π-electron approach, we compute the linear optical response of graphene QDs of various shapes and sizes with, and without, static external electric fields applied in the plane of QDs in various directions, and find that it is highly dependent upon the magnetic states of the QDs concerned. In particular, the nature of variation exhibited by the energy gaps corresponding to the up and down spins is different for the AFM and FM configurations of QDs. Therefore, we argue that the EA spectroscopy can prove to be a powerful alternative to convention magnetic measurements for determining the magnetic states of graphene QDs. Furthermore, selective manipulation of the spin-dependent splitting of gaps by an electric field in finite graphene nanostructures, namely, graphene QDs, can open up new frontiers in the design of graphene-based spintronic devices.

Remainder of this paper is organized as follows. In section II we briefly describe our theoretical methodology, while in section III our results are presented and discussed. Finally, in section IV we present our conclusions.

II. THEORETICAL METHODOLOGY

The symmetric structures considered here (*cf.* Fig. 1) include a rectangular QD with 54 carbon atoms (RQD-54), and a bowtie shaped QD with 38 atoms (BQD-38), both of which have D_{2h} symmetry. The QD with 40 atoms (GQD-40) exhibits lower C_{2v} symmetry, while those with 38, and 48 atoms (GQD-38 and GQD-48) are completely asymmetric. Quantum dots RQD-54, BQD-38, and GQD-38 have balanced sub-lattices, while GQD-40 and GQD-48 have imbalanced sub-lattices.

These calculations have been carried out using the effective π-electron Pariser-Parr-Pople (PPP) model

Hamiltonian,[27,28]

$$H = -\sum_{i,j,\sigma} t_{ij}\left(c^{\dagger}_{i\sigma}c_{j\sigma} + c^{\dagger}_{j\sigma}c_{i\sigma}\right) + U\sum_i n_{i\uparrow}n_{i\downarrow} + \sum_{i<j} V_{ij}(n_i - 1)(n_j - 1) \quad (1)$$

where $c^{\dagger}_{i\sigma}(c_{i\sigma})$ creates (annihilates) a π orbital of spin σ, localized on the ith carbon atom, while the total number of electrons with spin σ on atom i is indicated by $n_i = \sum_\sigma c^{\dagger}_{i\sigma}c_{i\sigma}$. Further, t_{ij}, U, and V_{ij}, denote hopping, onsite Coulomb repulsion, and long-range Coulomb interactions, respectively. Hopping matrix elements t_{ij} were restricted to nearest neighbor sites i and j, with their uniform value t_0 taken to be 2.4 eV, consistent with our earlier calculations on polymers,[29] polycyclic aromatic hydrocarbons,[30] and hydrogenated graphene nanofragments.[31] Coulomb interaction in the PPP model Hamiltonian are parametrized as per the Ohno relationship[32]

$$V_{ij} = U/\kappa_{i,j}(1 + 0.6117R^2_{i,j})^{1/2}, \quad (2)$$

where U, as described above, is the on-site electron-electron repulsion term, $\kappa_{i,j}$ represents the dielectric constant of the system which simulates the screening effects, and $R_{i,j}$ is the distance (in Å) between the ith and jth carbon atoms. In this work, we have performed calculations adopting "screened parameters", with U = 8.0 eV, $\kappa_{i,j}$= 2.0 ($i \neq j$), proposed initially by Chandross and Mazumdar, for studying the optical absorption in PPV,[33] and also used in several of our earlier works.[26,29,30,34–42] Present calculations were performed at the restricted Hartree-Fock (RHF) level for the non-magnetic states, and the unrestricted Hartree-Fock (UHF) level for the magnetic states, using a code developed in our group.[42] The details of the calculations are given extensively in our earlier works.[26,30,31,40,42]

All QDs considered here are assumed to lie in the x-y plane, with their longer dimension along the y axis. For EA calculations, the electric field is applied along the y-axis (transverse direction), x-axis (longitudinal direction), and diagonal directions in the x-y plane. All carbon-carbon bond lengths and bond angles have been fixed at 1.4 Å, and 120°, respectively.

III. RESULTS AND DISCUSSION

A. Ordering of states and HOMO-LUMO band gaps in the absence of electric field

In Table I we present the calculated difference in Hartree Fock (HF) total energy of the excited states, with respect to the ground state, and the HOMO-LUMO (H-L) band gaps for different magnetic phases of graphene QDs, in the absence of electric field. For the FM (AFM) phases, the z-component of the total spin (S_z) was taken to be 1 (0).

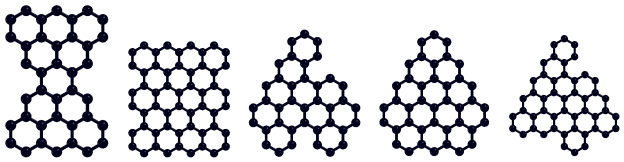

(a) BQD-38 (b) RQD-54 (c) GQD-38 (d) GQD-40 (e) GQD-48

Figure 1: Schematic diagrams of QDs considered in this work: (a) bowtie shaped (BQD-38), (b) rectangle shaped (RQD-54), while (c), (d), and (e) denote dots of lower symmetry GQD-38, GQD-40, and GQD-48, respectively.

QD	HF energy difference			H-L band-gap		
	E_{exc}- E_{gnd} (eV)			(eV)		
	AFM phase	FM phase	NM phase	AFM phase	FM phase	NM phase
RQD-54	0.00	0.47	1.79	3.97	2.76	0.90
BQD-38	0.00	0.49	4.72	4.24	3.25	0.58
GQD-38	0.00	0.88	0.59	4.02	2.94	2.47
GQD-40	0.83	0.00	2.01	2.47	4.39	0.55
GQD-48	0.78	0.00	2.08	2.49	4.03	0.51

Table I: Calculated difference in Hartree-Fock energy of the excited states with respect to the ground state and HOMO-LUMO band-gap for different magnetic phases of graphene QDs, in the absence of electric field. For the FM (AFM) phases z-component of the total spin (S_z) was taken to be 1 (0). For a given QD, E_{exc}(E_{gnd}), denotes the HF total energy of its higher (lower) energy magnetic state (AFM/FM)

An analysis of the energy difference (Table I) indicates that the QDs with balanced sublattices, i.e., equal number of A and B type atoms (RQD-54, BQD-38 and GQD-38), have the AFM state as the ground state, while the ones with imbalanced sublattices, namely, GQD-40 and GQD-48, have a ferromagnetic (FM) ground state. This is consistent with the Lieb's theorem[43] which states that the spin S of the ground state of the Hubbard model in neutral bipartite lattices is given by $2S = N_A - N_B$, where N_A and N_B represent the number of atoms constituting each sublattice. As far as the energetic ordering of various magnetic states is concerned, for RQD-54 and BQD-38, FM state follows the AFM ground state, with the non-magnetic (NM) state placed the highest. In comparison, for GQD-38, the excited state ordering is reversed. In case of GQD-40 and GQD-48, the AFM state appears next after the ground state, followed by the NM configuration.

The calculated H-L band gap (Table I) is largest for the ground-state configuration (namely AFM phase for RQD-54, BQD-38 and GQD-38 and FM state for GQD-

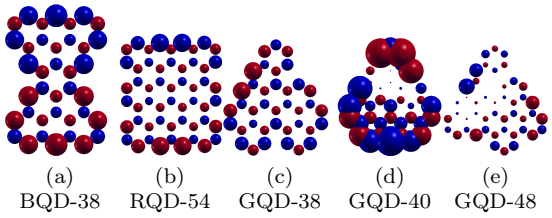

Figure 2: Spin-density plots of AFM configurations of: (a) BQD-38, (b) RQD-54, (c) GQD-38, (d) GQD-40, and (e) GQD-48, in the absence of electric field. The red and the blue spheres represent the two different spin orientations (up/down or α/β) of the carbon atoms.

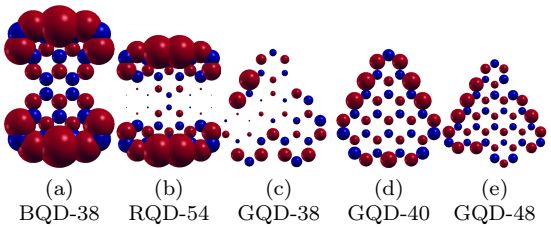

Figure 3: Spin-density plots of FM state of: (a) BQD-38, (b) RQD-54, (c) GQD-38, (d) GQD-40, and (e) GQD-48, in the absence of electric field. The red and the blue spheres represent the two different spin orientations (up/down or α/β) of the carbon atoms.

40 and GQD-48) while it is lowest for the NM state for all the QDs. Thus, it is possible to identify the ground-state magnetic coupling by analyzing the H-L band gap (optical band gap) of these QDs.

B. Spin-density plots of different magnetic phases of graphene quantum dots in the absence of electric field

1. *AFM phase*

Figure 2 represents spin-density plots of AFM configuration of BQD-38, RQD-54, GQD-38, GQD-40 and GQD-48, in the absence of electric field. The red and blue spheres represent the two different spin orientations (up/down or α/β) of the carbon atoms.

It is obvious from the figure that the spin densities corresponding to the two different spin orientations are localized on the opposite sides of the different quantum dots under consideration. This spatial asymmetry of the spin densities gives rise to local magnetism with zero net spin, expected for the AFM case.

2. *FM phase*

Figure 3 represents spin-density plots of FM state of BQD-38, RQD-54, GQD-38, GQD-40 and GQD-48, in the absence of electric field. It is observed that the spin density is largest on the zigzag edges and decreases rapidly from the zigzag edge to the middle of the QD. In addition, the spin density corresponding to (up (α) taken as majority spin) spin direction is more as compared to that of the other spin orientation giving rise to the FM character. In case of D_{2h} symmetry QDs (RQD-54 and BQD-38), the spin density is uniform at the opposite edges of the quantum dots. However, in case of lower symmetry (GQD-40) or completely asymmetric QDs (GQD-38 and GQD-48), the spin-density corresponding to majority spin orientation (up or α) is concentrated more on one side of the dot, as compared to the other side.

C. External electric field driven magnetic phase transitions of graphene quantum dots

Figure 4 presents the magnetic phase diagrams of BQD-38, RQD-54, GQD-38, GQD-40 and GQD-48, with the external electric field in the plane of the QDs being the control parameter. It is observed that there is no phase transition for QDs with balanced sublattices (BQD-38, RQD-54, GQD-38), under the influence of a longitudinal electric field (E_x). However, when these QDs are exposed to a transverse electric field (E_y), AFM order gets destroyed, resulting in an NM state. The intermediate FM phase for RQD-54 and BQD-38 is not achieved during the transition from AFM to NM state. Further, BQD-38, RQD-54, and GQD-38, undergo a phase change from AFM to NM configuration when subjected to an electric field in the xy plane, with unequal x/y components. Initially the NM phase of BQD-38 is stable when exposed to $E_y(\geq 0.28$ V/Å) but disappears at the instant E_x is switched on. However, at high values of E_y ($\geq$ 0.7 V/Å), the NM state is energetically stable under the influence of both E_x and E_y. In case of GQD-40, the ground state (FM) remains stable, while a phase transition occurs from the first excited state (AFM) to the second excited state (NM), when a low strength electric field is applied in any direction in the xy plane, as depicted in the inset of the phase diagram of GQD-40.

The ground state (FM) remains unchanged when GQD-40 is exposed to a purely longitudinal field. However, at higher values of E_y ($\geq$0.54 V/Å), a phase change from the ground state (FM) to NM configuration is observed. For this magnitude of E_y, the NM configuration is destroyed, at the instant E_x is also applied. However, the NM phase becomes energetically stable at this value of E_y, for higher strength of E_x ($\geq$1.57 V/Å). The ground state (FM) of GQD-48, on the other hand, undergoes a phase transformation to the AFM phase, with the application of an electric field in any direction in the xy plane. In this case, in contrast to GQD-40, an initial phase change between the excited states is not observed. Thus, direction of electric field plays an important role in the tuning of phase transitions exhibited by QDs.

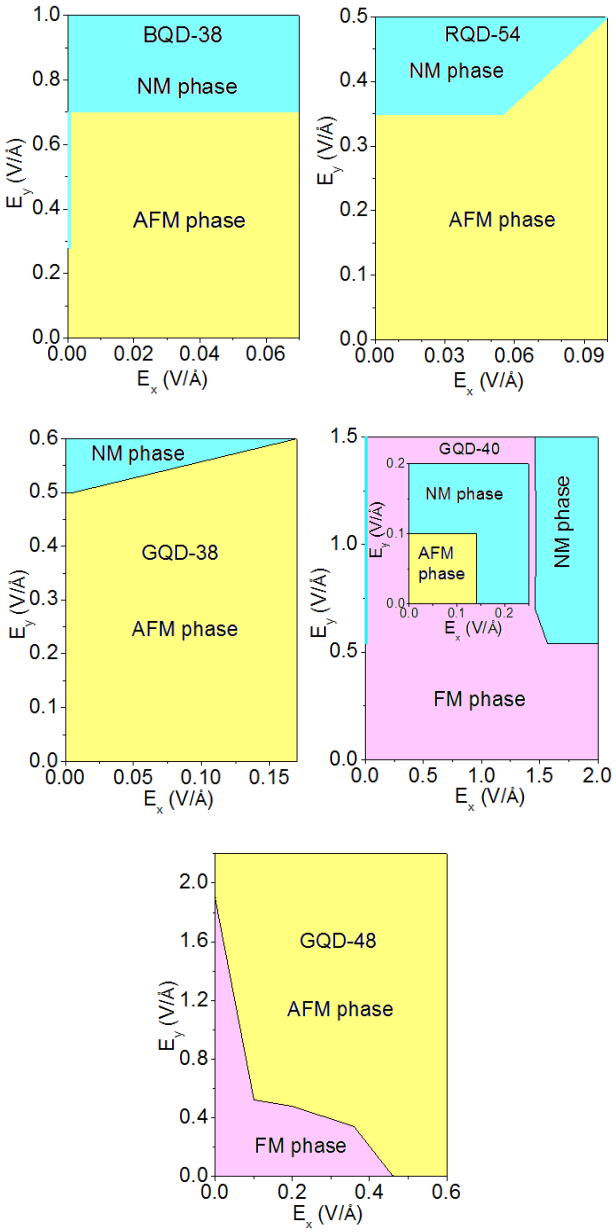

Figure 4: Phase diagrams of the different magnetic phases of BQD-38, RQD-54, GQD-38, GQD-40 and GQD-48 in the presence of electric field. The inset of GQD-40 represents a phase transition from the first excited state (AFM) to the second excited state (NM).

D. Dependence of spin-polarized band-gaps of AFM and FM phases on external electric field

Figure 5 represents the variation in the spin-polarized H-L band-gaps of AFM and FM phases of QDs, as functions of transverse electric field. The H-L band-gap corresponding to the two different spin-orientations (α and β) are degenerate in the absence of electric field, for both the AFM, and the FM configurations. In case of the AFM phase, the application of electric field results in a splitting of the band-gaps for up and down spins. The band-gaps of spin-down (β) electrons decrease uniformly, while those of up-spin (α) electrons increases. However, the band-gap of β electrons never closes due to finite-size effect of the quantum dots.[3] Thus, the behavior of the spin-polarized band-gap under the influence of an external electric field is not exactly half-metallic. With the increasing electric field, the band-gap splitting decreases, and eventually the gaps for α and β spins again become degenerate for all the QDs considered, except GQD-48. The band-gap splitting in AFM state arises due to the spatial localization of the spin densities corresponding to α and β spins at the opposite edges of the quantum dot (Fig. 2). The application of electric field leads to a spin transfer, due to charge transfer, between the opposite corners of QDs, resulting in a decrease in spatial localization of spins, and the band-gap splitting. The degeneracy of the spin-polarized band gaps at higher electric fields is due to phase transition of AFM state to NM state. Sharp drops in the band gaps of RQD-54 and BQD-38 leading to the spin degeneracy are due to the large difference between the band gaps of the AFM and NM states (Table I) of these QDs. This splitting of the H-L band-gap is always evident when the QDs are subjected to an in-plane transverse or diagonal electric field, while it is absent for an in-plane longitudinal electric field for BQD-38, RQD-54, GQD-38, and GQD-40. The band-gap splitting is more pronounced for QDs (RQD-54, BQD-38) with high symmetry (D_{2h} symmetry), as compared to QDs (GQD-38, GQD-40 and GQD-48) which exhibit either a lower symmetry (C_{2v} symmetry), or are completely asymmetric.

For FM configurations, the H-L band-gap corresponding to α and β spins remains degenerate under the influence of electric field in any direction, for D_{2h} symmetry QDs (RQD-54 and BQD-38), and it decreases with the increasing field. However, for lower symmetry (GQD-40 with C_{2v} symmetry) or asymmetric QDs (GQD-38 and GQD-48), the electric field splits the gap for the two spin orientations. With the increasing field strength, the gap corresponding to one spin orientation (α) decreases more rapidly as compared to that of the other spin (β). This H-L gap splitting always occurs in the presence of in-plane transverse and diagonal electric fields, while it is absent for longitudinal electric field for GQD-40. This band-gap splitting in the FM phase is due to the greater concentration of spin-density of the same spin flavour at one side, as compared to the other side of the quantum dot (Fig. 3). Further, in contrast to the AFM phase, the gaps corresponding to the α and β spins in the FM state never become degenerate, even for extremely high values of the electric field. This unique property of tuning of the spin-dependent band-gap of AFM and FM arrangements of QDs by electric fields of different strengths and alignments can be effectively used in the field of spintronics.

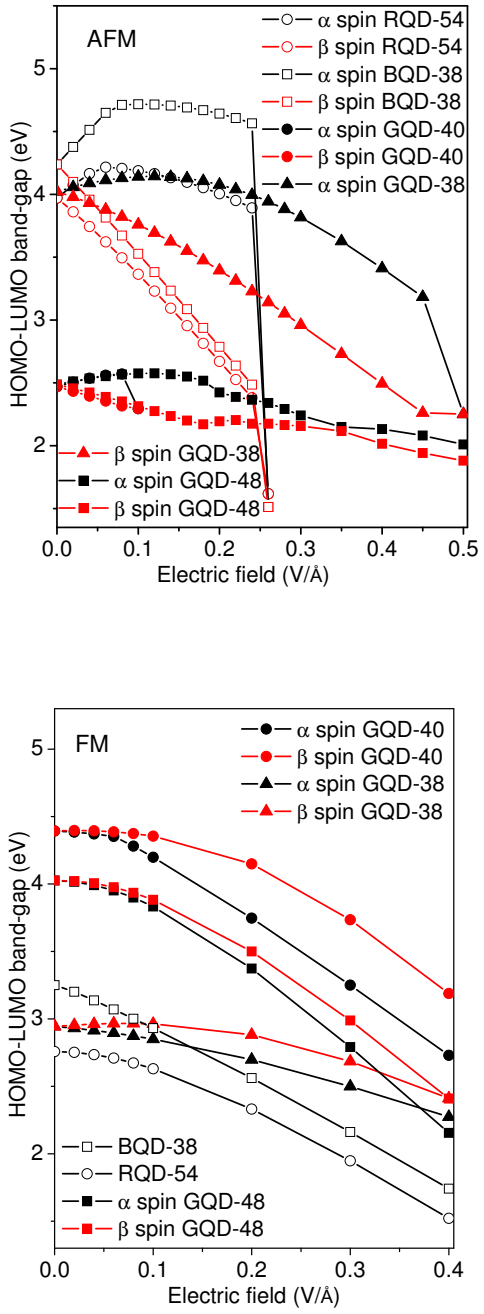

Figure 5: Variation of spin-polarized HOMO-LUMO band-gap of AFM and FM phase of QDs as a function of an in-plane transverse electric field.

E. Electroabsorption spectra of various magnetic phases of QDs

Next, we analyze the EA spectra, i.e., optical absorption spectra as a function of external electric field, of various magnetic phases of QDs. The salient features exhibited by the EA spectra of the AFM and FM phases of BQD-38, RQD-54, GQD-40, GQD-48 and GQD-38 indicate that, in the absence of a magnetic phase diagram, the EA spectra is self-sufficient to predict not only the magnetic ground state, but also the states attained by the QDs after the phase transition. Next, we discuss the calculated EA spectra of different classes of QDs considered in this work.

1. *Highly symmetric QDs with D_{2h} symmetry*

The EA spectra of the AFM and FM phases of highly symmetric QDs with D_{2h} symmetry (BQD-38 and RQD-54) corresponding to transverse, longitudinal and diagonal electric field, are presented in Figs. 6, 7 and 8, respectively. Salient features of the calculated absorption spectra are as follows.

1. The EA spectrum of AFM phase of BQD-38 and RQD-54 exhibits a spin-sensitive split on applying transverse electric fields. (Fig. 6(a) and Fig. 6(d)). However, this spin splitting of the EA spectrum is not observed, in the presence of transverse electric field, for the FM phases of BQD-38 (6 (c)) and RQD-54 (Fig. 6 (f)). Thus, this distinctive feature of the EA spectrum, in the presence of transverse electric field, can be used to identify the ground state magnetic configuration of these QDs.

2. At higher values of transverse electric fields (E_y≈0.3 V/Å), the spin splitting of the EA spectrum of the AFM phase of BQD-38 and RQD-54 vanishes (pink solid line in figs. 6 (b) and 6 (e)), indicating a phase transition. In order to identify the state (FM or NM) attained by the QDs after this phase transition, energy shifts of the EA spectra with increasing transverse electric field (E_y>0.3 V/Å) are analyzed. If the AFM phase undergoes a phase change to NM state at E_y≈0.3 V/Å, the EA spectrum gets blue shifted at electric fields E_y>0.3 V/Å (see orange dashed lines in Figs. 6 (b) and 6 (e) at E_y=0.4 V/Å). On the other hand, if the FM state is reached after the phase transition, the EA spectrum gets red shifted at electric fields E_y>0.3 V/Å (see green dotted lines in Figs. 6 (b) and 6 (e), at E_y=0.4 V/Å). Since, the EA spectrum of the AFM configuration at E_y=0.4 V/Å exhibits a blue-shift and coincides with the EA spectrum of the NM state at E_y=0.4 V/Å(figs. 6 (b) and 6 (e) for BQD-38 and RQD-54, respectively), it implies that the AFM phase undergoes a phase transition to the NM state, as also predicted by their phase diagrams (Fig. 4).

3. The EA spectra of the AFM phases of BQD-38 and RQD-54 do not exhibit a spin-sensitive split on the application of longitudinal electric fields (Fig. 7). However, these spectra do exhibit split corresponding to opposite spin orientations, when perturbed by an in-plane diagonal electric field (Fig.

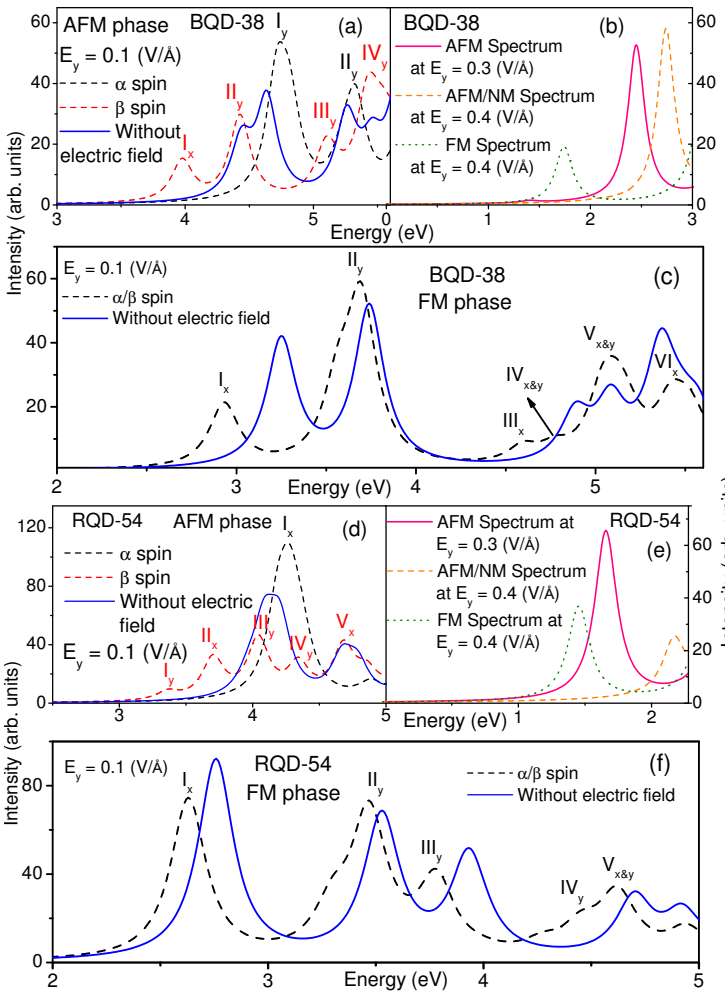

Figure 6: Computed EA spectrum broadened with a uniform line-width of 0.1 eV for the (a) AFM phase of BQD-38 (b) AFM (pink solid line) at E_y=0.3 V/Å, NM (orange dashed line) and FM phase (green dotted line) at E_y=0.4 V/Å, of BQD-38 (c) FM phase of BQD-38 (d) AFM phase of RQD-54 (e) AFM (pink solid line) at E_y=0.3 V/Å, NM (orange dashed line) and FM phase (green dotted line) at E_y=0.4 V/Å, of RQD-54 and (f) FM phase of RQD-54. The red and black dotted lines indicate the optical spectra for spin-down (β spin) and spin-up (α spin) orbitals, respectively, in the presence of E_y= 0.1 V/Å. The blue solid line indicates the optical spectrum in the absence of electric field. Peak labels imply peak numbers, with the subscripts indicating the polarization directions.

8). Thus, we conclude that the presence of a transverse component in the external electric field is essential for spin splitting to be observed in the AFM phase EA spectra of these QDs.

4. In case of the FM states of BQD-38 and RQD-54, the EA spectra do not exhibit any spin-sensitive split on application of in-plane longitudinal and diagonal electric fields. Thus, spin-sensitive splitting of the optical spectrum, on the application of electric field in any direction, is not possible for the FM phase of BQD-38 and RQD-54.

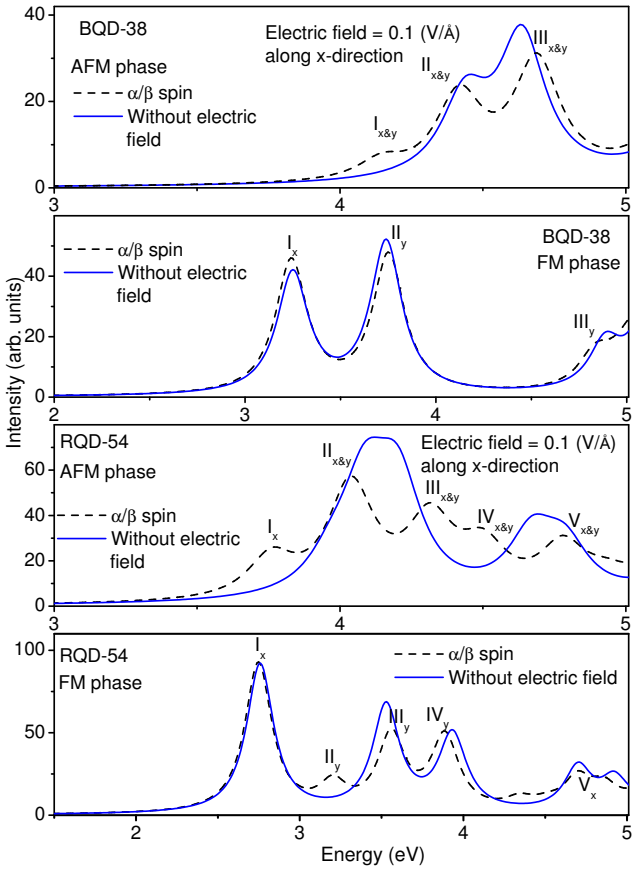

Figure 7: Computed EA spectrum broadened with a uniform line-width of 0.1 eV for the AFM and FM phases of BQD-38 and RQD-54. The black dotted line indicates the spectra for both the spin-up (α spin) and spin-down (β spin) electrons, in the presence of an in-plane longitudinal electric field of 0.1 V/Å. The blue solid line indicates the absorption spectrum in the absence of electric field. Peak labels imply peak numbers, with the subscripts indicating the polarization directions.

2. *Low symmetry QDs*

Calculated EA spectra of the AFM and FM phases of QDs with C_{2v} symmetry (GQD-40), and the ones with no symmetry (GQD-38 and GQD-48), corresponding to transverse, longitudinal and diagonal electric field, are presented in Figs. 9, 10, 11, 12, 13 and 14. Main features of the spectra are summarized below.

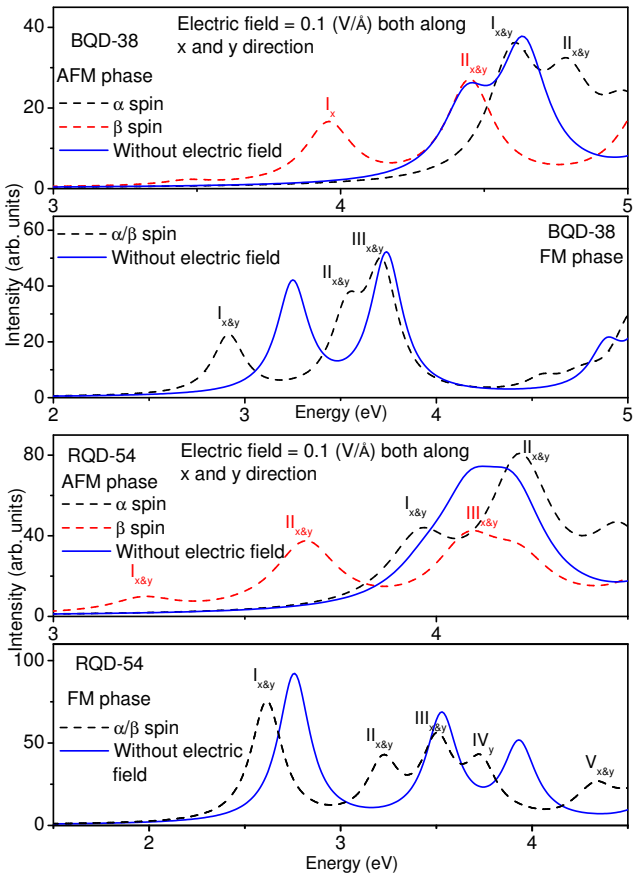

Figure 8: Computed EA spectrum broadened with a uniform line-width of 0.1 eV for the AFM and FM phases of BQD-38 and RQD-54. The red and black dotted lines indicate the spectra for spin-down (β spin) and spin-up (α spin) electrons, respectively, in the presence of an in-plane diagonal electric field of 0.1 V/Å. Peak labels imply peak numbers, with the subscripts indicating the polarization directions.

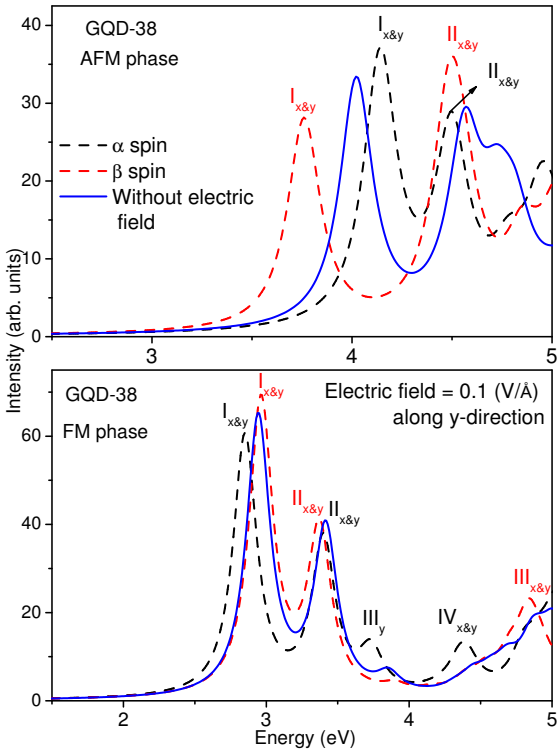

Figure 9: Computed EA spectrum broadened with a uniform line-width of 0.1 eV for the AFM and FM phases of GQD-38. The red and black dotted lines indicate the optical spectra for spin-down (β spin) and spin-up (α spin) electrons, respectively, in the presence of transverse electric field. The blue solid line indicates the optical spectrum in the absence of electric field. Peak labels imply peak numbers, with the subscripts indicating the polarization directions.

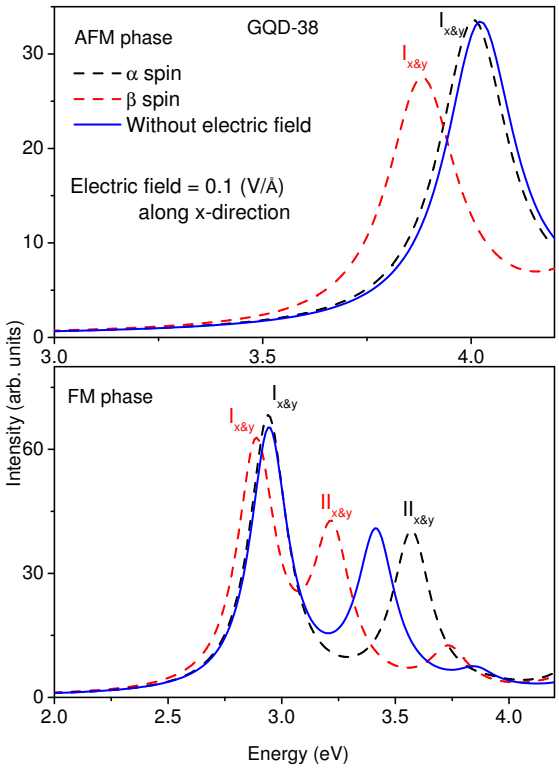

Figure 10: Computed EA spectrum broadened with a uniform line-width of 0.1 eV for the AFM and FM phases of GQD-38. The red and black dotted lines indicate the optical spectra for spin-down (β spin) and spin-up (α spin) electrons, respectively, in the presence of longitudinal electric field. The blue solid line indicates the optical spectrum in the absence of electric field. Peak labels imply peak numbers, with the subscripts indicating the polarization directions.

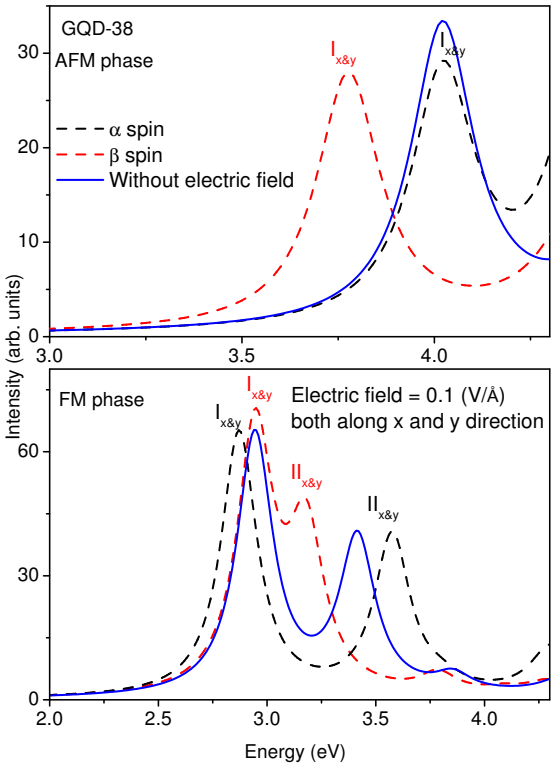

Figure 11: Computed EA spectrum broadened with a uniform line-width of 0.1 eV for the AFM and FM phases of GQD-38. The red and black dotted lines indicate the optical spectra for spin-down (β spin) and spin-up (α spin) electrons, respectively, in the presence of a diagonal electric field. The blue solid line indicates the optical spectrum in the absence of electric field. Peak labels imply peak numbers, with the subscripts indicating the polarization directions.

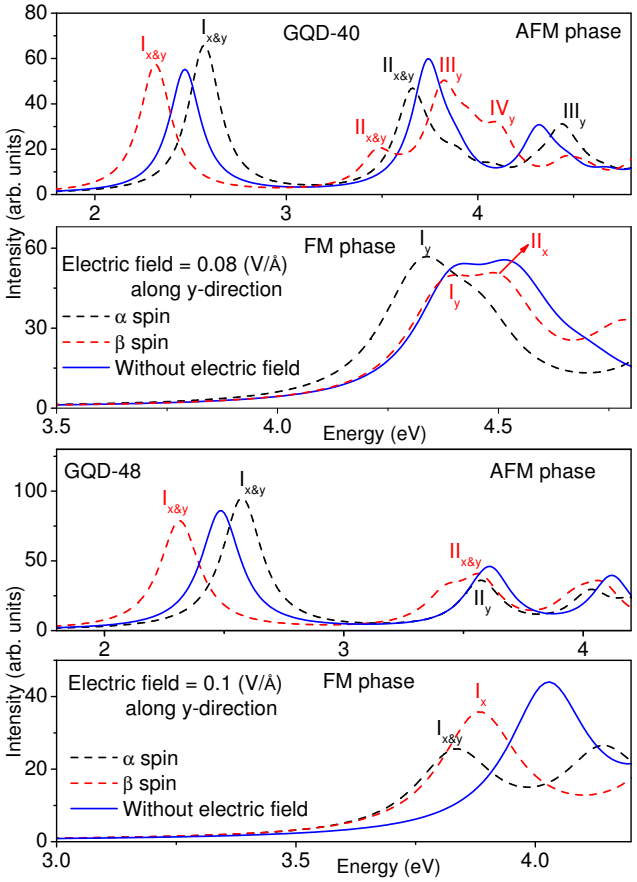

Figure 12: Computed EA spectrum broadened with a uniform line-width of 0.1 eV for the AFM and FM phases of GQD-40 and GQD-48. The red and black dotted lines indicate the optical spectra for spin-down (β spin) and spin-up (α spin) electrons, respectively, in the presence of a transverse electric field. The blue solid line indicates the optical spectrum in the absence of electric field. Peak labels imply peak numbers, with the subscripts indicating the polarization directions.

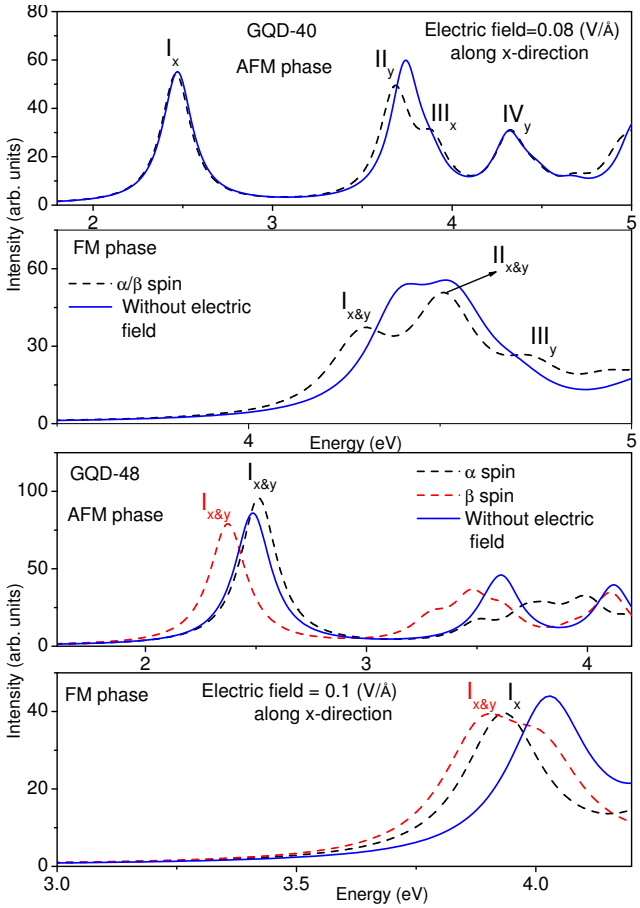

Figure 13: Computed EA spectrum broadened with a uniform line-width of 0.1 eV for the AFM and FM phases of GQD-40 and GQD-48. The red and black dotted lines indicate the optical spectra for spin-down (β spin) and spin-up (α spin) electrons, respectively, in the presence of a longitudinal electric field. The blue solid line indicates the optical spectrum in the absence of electric field. Peak labels imply peak numbers, with the subscripts indicating the polarization directions.

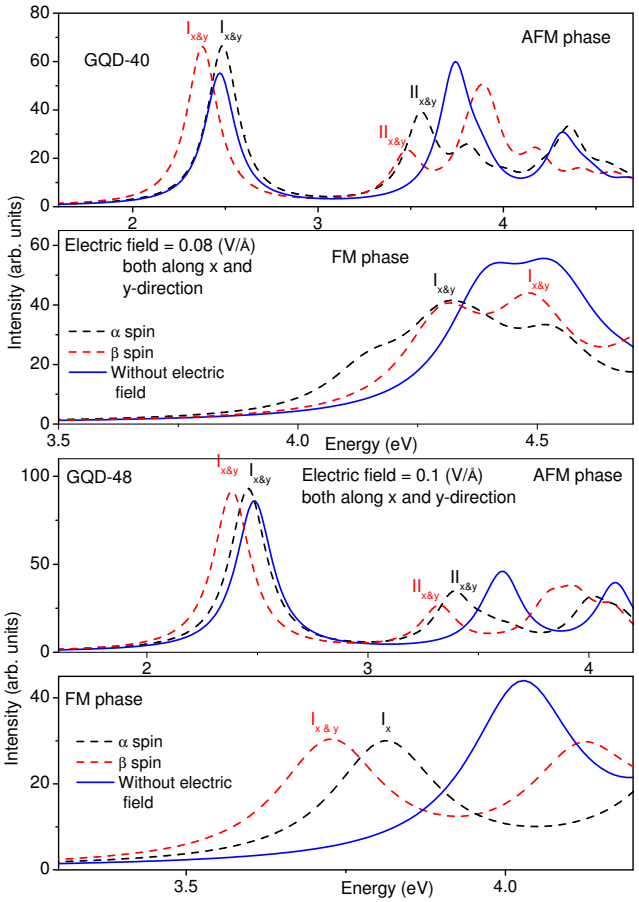

Figure 14: Computed EA spectrum broadened with a uniform line-width of 0.1 eV for the AFM and FM phases of GQD-40 and GQD-48. The red and black dotted lines indicate the optical spectra for spin-down (β spin) and spin-up (α spin) electrons, respectively, in the presence of diagonal electric field. The blue solid line indicates the optical spectrum in the absence of electric field. Peak labels imply peak numbers, with the subscripts indicating the polarization directions.

1. The EA spectra of both the AFM and FM phases of QDs of C_{2v} (GQD-40), and totally asymmetric QDs (GQD-38 and GQD-48), exhibit spin splitting (Figs. 9 and 12), in the presence of transverse electric field. In case of the AFM state, the EA spectra for α and β spins are shifted in opposite directions with the increasing field strength, with the spectra for α/β spins exhibiting blue/red shifts, with respect to the absorption spectra in the absence of electric field. However, for the FM phase, the EA spectra for both types of spins get red shifted with the increasing field. This marked difference exhibited by the EA spectrum of AFM and FM states can be used to characterize the magnetic ground states of QDs of lower symmetries.

2. Absorption spectra of FM phase of completely asymmetric GQDs (GQD-38 and GQD-48) exhibit maximum sensitivity towards electric fields, and split for two spin orientations when exposed to an in-plane electric field in any direction (Figs. 9, 10, 11, 12, 13 and 14). However, the EA spectra of the AFM and FM states of QDs of C_{2v} symmetry (GQD-40), similar to the behavior discussed earlier for QDs with D_{2h} symmetry, does not exhibit a spin-sensitive split on application of a longitudinal electric field (Fig. 13). This distinctive feature displayed by the EA spectrum can be used to distinguish the low symmetry QDs, from totally asymmetric ones.

3. In addition, when the magnetic ground states of GQD-38 and GQD-40 undergo a phase transition to the NM phase, the spin-dependent optical splitting vanishes. For the AFM phase, the field-induced splitting of the EA spectrum for two spin orientations is more pronounced in the lower energy region, because, the higher energy peaks are due to excitations from orbitals further away from the Fermi level, which exhibit decreasing spin polarity. For all the QDs studied, the peak patterns for the two spin orientations for AFM/FM states are quite distinct, along with their relative intensities, even at low values of the applied electric field. Thus, it is possible to identify the magnetic ground state, as well as the energy states attained after electric-field driven phase transitions, by means of EA spectroscopy.

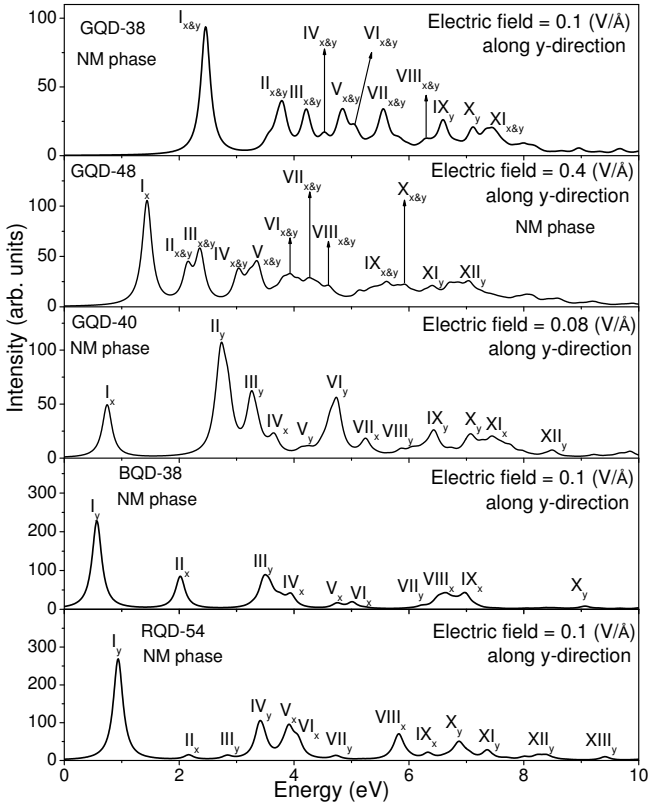

Figure 15: Computed optical absorption spectra for NM phases of GQD-38, GQD-48, GQD-40, BQD-38, and RQD-54 in the presence of an in-plane transverse electric field. The computed spectrum has been broadened with a uniform line-width of 0.1 eV. Peak labels imply peak numbers, with the subscripts indicating the polarization directions.

The EA spectra for the NM phase, in the presence of an in-plane transverse electric field, for all the QDs considered in this work has been given in Fig. 15. It is observed that the EA spectra for the NM phase is drastically different from the EA spectra of the magnetic phases (AFM and FM). Thus, we expect that EA spectra can be used as to successfully differentiate various magnetic and nonmagnetic states of graphene quantum dots.

IV. CONCLUSIONS

In this work, calculations on different magnetic states (AFM and FM) of graphene QDs have indicated that energy gaps of these magnetic states exhibit spin dependence. Also, the manner in which the spin-dependent energy gaps vary, when exposed to a suitably aligned electric field, is distinct for the AFM and FM configurations of QDs. This empowers us to manipulate the band gaps by an external electric field, which is of fundamental significance in spintronics. Additionally, our studies have elucidated the correlation between spin density, and optical band-gap splitting. It has been shown that energy band-gap splitting for the AFM phase arises due to spatial localization of spin density corresponding to the two distinct spin orientations on the opposite edges of the quantum dots. In contrast, higher concentration of spin density associated with same spin in one region of the QD, as compared to the other regions, is responsible for band-gap splitting in the FM state. We have then shown that the magnetic states of QDs undergo phase transitions on application of an electric field. Furthermore, we have demonstrated that the EA spectra of different magnetic states of QDs have distinct footprints (peak pattern as well as nature of peak shifts). Thus, by studying the variation of the EA spectra as a function of the field strength, one can efficiently distinguish different magnetic states of QDs. We hope that our findings will create ways to realize spintronic devices based on graphene QDs, in the near future.

* tista.basak@nmims.edu, shukla@phy.iitb.ac.in

[1] Y.-W. Son, M. L. Cohen, and S. G. Louie, Nature **444**, 347 (2006).
[2] L. A. Agapito, N. Kioussis, and E. Kaxiras, Phys. Rev. B **82**, 201411 (2010).
[3] H. Zheng and W. Duley, Phys. Rev. B **78**, 155118 (2008).
[4] S. Bhowmick and V. B. Shenoy, The Journal of Chemical Physics **128**, 244717 (2008).
[5] A. Zhou, W. Sheng, and S. J. Xu, Applied Physics Letters **103**, 133103 (2013).
[6] W.-L. Ma and S.-S. Li, Phys. Rev. B **86**, 045449 (2012).
[7] H. Sahin, R. T. Senger, and S. Ciraci, Journal of Applied Physics **108**, 074301 (2010).
[8] W. L. Wang, S. Meng, and E. Kaxiras, Nano Letters **8**, 241 (2008).
[9] H. Feldner, Z. Y. Meng, A. Honecker, D. Cabra, S. Wessel, and F. F. Assaad, Phys. Rev. B **81**, 115416 (2010).
[10] Z. Z. Zhang, K. Chang, and F. M. Peeters, Phys. Rev. B **77**, 235411 (2008).
[11] H. Zheng and W. Duley, Phys. Rev. B **78**, 045421 (2008).
[12] M. Zarenia, A. Chaves, G. A. Farias, and F. M. Peeters, Phys. Rev. B **84**, 245403 (2011).
[13] A. D. Güçlü and P. Hawrylak, Phys. Rev. B **87**, 035425 (2013).
[14] J. Fernández-Rossier and J. J. Palacios, Phys. Rev. Lett. **99**, 177204 (2007).
[15] L. A. Agapito and N. Kioussis, The Journal of Physical Chemistry C **115**, 2874 (2011).
[16] A. D. Güçlü, P. Potasz, and P. Hawrylak, Phys. Rev. B **82**, 155445 (2010).
[17] K. Szałowski, Phys. Rev. B **90**, 085410 (2014).

[18] N. Tombros, C. Jozsa, M. Popinciuc, H. T. Jonkman, and B. J. van Wees, Nature **448**, 571 (2007).
[19] O. V. Yazyev and M. I. Katsnelson, Phys. Rev. Lett. **100**, 047209 (2008).
[20] W. Han, K. Pi, W. Bao, K. M. McCreary, Y. Li, W. H. Wang, C. N. Lau, and R. K. Kawakami, Applied Physics Letters **94**, 222109 (2009).
[21] T.-Y. Yang, J. Balakrishnan, F. Volmer, A. Avsar, M. Jaiswal, J. Samm, S. R. Ali, A. Pachoud, M. Zeng, M. Popinciuc, G. Güntherodt, B. Beschoten, and B. Özyilmaz, Phys. Rev. Lett. **107**, 047206 (2011).
[22] L. Chen, L. Guo, Z. Li, H. Zhang, J. Lin, J. Huang, S. Jin, and X. Chen, Sci. Rep. **3**, 2599 (2013).
[23] G. Z. Magda, X. Jin, I. Hagymasi, P. Vancso, Z. Osvath, P. Nemes-Incze, C. Hwang, L. P. Biro, and L. Tapaszto, Nature **514**, 608 (2014).
[24] M. Kiguchi, K. Takai, V. L. J. Joly, T. Enoki, R. Sumii, and K. Amemiya, Phys. Rev. B **84**, 045421 (2011).
[25] K. Suenaga and M. Koshino, Nature **468**, 1088 (2010).
[26] K. Gundra and A. Shukla, Phys. Rev. B **83**, 075413 (2011).
[27] J. A. Pople, Trans. Faraday Soc. **49**, 1375 (1953).
[28] R. Pariser and R. G. Parr, J. Chem. Phys. **21**, 767 (1953).
[29] P. Sony and A. Shukla, Phys. Rev. B **71**, 165204 (2005).
[30] K. Aryanpour, A. Shukla, and S. Mazumdar, The Journal of Chemical Physics **140**, 104301 (2014).
[31] T. Basak, H. Chakraborty, and A. Shukla, Phys. Rev. B **92**, 205404 (2015).
[32] K. Ohno, Theoretica chimica acta **2**, 219 (1964).
[33] M. Chandross and S. Mazumdar, Phys. Rev. B **55**, 1497 (1997).
[34] P. Sony and A. Shukla, The Journal of Chemical Physics **131**, 014302 (2009).
[35] H. Chakraborty and A. Shukla, The Journal of Physical Chemistry A **117**, 14220 (2013).
[36] K. Aryanpour, A. Roberts, A. Sandhu, R. Rathore, A. Shukla, and S. Mazumdar, The Journal of Physical Chemistry C **118**, 3331 (2014).
[37] H. Chakraborty and A. Shukla, The Journal of Chemical Physics **141**, 164301 (2014).
[38] A. Shukla, Phys. Rev. B **65**, 125204 (2002).
[39] A. Shukla, Phys. Rev. B **69**, 165218 (2004).
[40] K. Gundra and A. Shukla, Phys. Rev. B **84**, 075442 (2011).
[41] P. Sony and A. Shukla, Phys. Rev. B **75**, 155208 (2007).
[42] P. Sony and A. Shukla, Computer Physics Communications **181**, 821 (2010).
[43] E. H. Lieb, Phys. Rev. Lett. **62**, 1201 (1989).